Geophysical Research Letters

RESEARCH LETTER
10.1029/2020GL091980

Key Points:

- Global tropical cyclone frequency is found to be proportional to the Coriolis parameter at the intertropical convergence zone
- The same proportionality obtained from aquaplanet simulations also applies to tropical cyclone frequency on the observed Earth
- Many tropical cyclones occur even when the location of maximum sea surface temperature is shifted into the midlatitudes

Supporting Information:

- Supporting Information S1
- Figure S1
- Figure S2
- Figure S3
- Figure S4
- Figure S5
- Figure S6
- Figure S7
- Figure S8
- Figure S9
- Figure S10
- Figure S11
- Figure S12
- Figure S13
- Movie S1
- Movie S2

Correspondence to:

A. C. Burnett,
acb18@stanford.edu

Citation:

Burnett, A. C., Sheshadri, A., Silvers, L. G., & Robinson, T. (2021). Tropical cyclone frequency under varying SSTs in aquaplanet simulations. *Geophysical Research Letters*, *48*, e2020GL091980. https://doi.org/10.1029/2020GL091980

Received 4 DEC 2020
Accepted 5 FEB 2021

Tropical Cyclone Frequency Under Varying SSTs in Aquaplanet Simulations

Adam C. Burnett[1], Aditi Sheshadri[1], Levi G. Silvers[2,3,4,5], and Thomas Robinson[2,6]

[1]Department of Earth System Science, Stanford University, Stanford, CA, USA, [2]Geophysical Fluid Dynamics Laboratory, Princeton, NJ, USA, [3]Atmospheric and Oceanic Sciences Program, Princeton University, Princeton, NJ, USA, [4]School of Marine and Atmospheric Sciences, Stony Brook University, Stony Brook, NY, USA, [5]Now at School of Marine and Atmospheric Sciences, Stony Brook University, Stony Brook, NY, USA, [6]SAIC, Princeton, NJ, USA

Abstract Global tropical cyclone (TC) frequency is investigated in a 50-km-resolution aquaplanet model forced by zonally symmetric sea surface temperature (SST). TC frequency per unit area is found to be proportional to the Coriolis parameter at the intertropical convergence zone (ITCZ), as defined by the latitude of maximum precipitation. As the latitude of maximum SST is shifted northward from the equator, the precipitation maximum moves northward and TC frequency increases. When the SST maximum is shifted northward past 25°N, the precipitation maximum remains between 15°N and 20°N, and TC frequency per unit area is approximately constant. When applied to observed precipitation and SST data, the same scaling captures a substantial fraction of observed TCs. Results suggest that future changes in TC activity will be modulated by changes in the large-scale circulation, and in particular that the ITCZ location is an important determinant of the number of TCs.

Plain Language Summary Tropical cyclones (TCs), including hurricanes, can be extremely destructive and costly, so it is important to know how often they will occur in the future. Earth presently experiences about 90 TCs per year, but whether this number will change due to climate change is uncertain. A theory describing what physical quantities determine the global number of TCs would improve predictions of future TC frequency. In this study, we search for possible ingredients in such a theory by using a simplified global climate model without seasons or land. When we shift the temperature distribution of the ocean surface northward, the TC frequency changes. Through statistical analysis and physical reasoning, these changes in global TC frequency are explained by two physical quantities. One of these quantities depends on the position of the intertropical convergence zone, defined in this study as the latitude of maximum rainfall in the tropics. The other quantity depends on the latitude of maximum ocean surface temperature. These results suggest that any physical theory describing global TC frequency must be consistent with these two quantities. This finding marks a step toward more complete understanding, and improved future projections, of TC frequency.

1. Introduction

The frequency of tropical cyclones (TCs) on Earth is consistent at 90 ± 10 per year (Emanuel, 2006), but no large-scale dynamical theory exists to explain this observation. Studies projecting changes in TC frequency under climate change have produced conflicting results (e.g., Emanuel, 2013; Held & Zhao, 2011). Various empirical indices predicting TC activity, such as potential intensity (Emanuel, 1986) and genesis potential (Camargo et al., 2007), apply well to the present climate, but when used to project future TC frequency, different genesis indices can make opposite predictions (Camargo et al., 2014). A dynamical theory predicting TC frequency from large-scale planetary parameters would provide fundamental insight into these unresolved problems.

Aquaplanet experiments, in which a general circulation model (GCM) is run with no land or seasonality, provide simplified systems suitable for testing large-scale predictions (Merlis & Held, 2019). GCMs now have sufficiently high resolution, 50 km or higher, to produce TC-like storms. These simulated TCs are weaker than observed TCs, but their qualitative behavior is similar (Shaevitz et al., 2014). Several studies have used aquaplanet experiments and other global-scale simulations to investigate dynamical controls of TC frequency (e.g., Ballinger et al., 2015; Chavas & Reed, 2019; Held & Zhao, 2011; Hsieh et al., 2020;

Merlis et al., 2013; Zhao & Held, 2012; Zhao et al., 2009). Of these studies, Merlis et al. (2013) is the first to formulate a quantitative scaling for the global frequency of TCs. They propose that the annual number N of TCs in a model experiment is a function of the latitude of the intertropical convergence zone (ITCZ) and the mean tropical sea surface temperature (SST), with increasing TC frequency as the ITCZ is shifted northward (Merlis et al., 2013). Ballinger et al. (2015) also simulate TCs in a 50-km-resolution aquaplanet model in an effort to understand the dependence of N. They conclude that changes in the SST profile shift the ITCZ, which causes changes in TC activity, with TC frequency increasing as the latitude of SST maximum is moved northward from 10°N to 13°N to 16°N. Other studies have investigated what sets the ITCZ position in an aquaplanet (e.g., Byrne et al., 2018; Möbis & Stevens, 2012), linking ITCZ-based theories of TC frequency with more fundamental understanding. Meanwhile, Chavas and Reed (2019) performed uniform-SST aquaplanet simulations, varying planetary size and rotation rate, and found that TC frequency increases linearly with the value of the Coriolis parameter in simulations without a local SST maximum and hence without an ITCZ. Combined with the findings of Merlis et al. (2013), these results suggest the hypothesis, which we test in this study, that global TC frequency is a linear function of the Coriolis parameter at the ITCZ.

2. Methods

2.1. Aquaplanet Model Configuration

In this study, we investigate TC activity in a 50-km-resolution aquaplanet configuration of the Geophysical Fluid Dynamics Laboratory (GFDL) Atmosphere Model 4.0 (AM4.0; Zhao et al., 2018a,b), with a fixed, zonally symmetric SST distribution. AM4.0 was developed at GFDL and used as part of Coupled Model Intercomparison Project Phase 6 (CMIP6; Eyring et al., 2016). Because this study is focused on TCs, the ITCZ, and the location of the SST maximum, we use an aquaplanet version of AM4.0, which we call AM4.0-Aqua. Using an aquaplanet model also allows us to utilize short spin-up times. AM4.0-Aqua differs from the default AM4.0 in several ways, as follows. No land is present, and the lower boundary simply provides a source of moisture and heat and a sink of momentum. The prognostic aerosol of AM4.0 is turned off and the cloud condensation nuclei concentration number is prescribed as 10^8 m^{-3}. Earth-like parameters are used for the rotation and insolation with a perpetual equinox. Ozone is prescribed as zonally uniform but varies meridionally and vertically. The greenhouse gases are uniformly mixed and follow Aqua-Planet Experiment (APE) protocol as specified by Neale and Hoskins (2000) and Williamson et al. (2012). The SST is prescribed as a function that varies only with latitude. Our experiments with the SST maximum at the equator and 5°N use the same SST distributions as the "Control" and "Control-5N" experiments, respectively, defined in Equations 1 and 4 of Neale and Hoskins (2000). Our other experiments use the same equation as the "Control-5N" experiment but with different latitudinal shifts, as shown in Figure S1. When the latitude of the SST maximum is shifted sufficiently far northward, the minimum SST north of the SST maximum remains above 0°C.

AM4.0 uses the GFDL Finite-Volume Cubed-Sphere Dynamical Core (FV3) (Harris & Lin, 2013; Putman & Lin, 2007). The default aquaplanet based on AM4.0 that was used as part of CMIP6 has a grid spacing of approximately 100 km (C96). Here we use a smaller grid spacing of approximately 50 km (C192). This configuration is run with the same physics parameterizations for radiation, convection, large-scale cloud, microphysics, and turbulence as AM4.0 (see Zhao et al., 2018b and references therein). The model top is at 1 hPa, with 33 vertical levels. The kilometer closest to the surface is resolved by eight levels. A sponge layer is present between 1 and 8 hPa. Model runs were conducted on a Cray XC40 named Gaea at the Oak Ridge National Laboratory and compiled with the Intel compiler version 16.0.3.210 for consistency with AM4.0.

A total of 13 model runs were analyzed, each with the SST maximum at a different latitude, varying by 5° increments from 0° to 60°N. Each model run was integrated for 5 years, with the first 2 months of data discarded for spin-up. Figure S2 shows plots of globally integrated water vapor mass as a function of time for four different simulations. These plots illustrate that a steady-state value is reached within a spin-up time of 2 months.

The location of the ITCZ in each model run is identified using the precipitation distribution. The precipitation, output at monthly intervals, is averaged zonally and temporally over the duration of each experiment. The center of the ITCZ is identified as the first local precipitation maximum north of the equator that has

at least half the value of the global maximum. With the exception of the experiment with SST maximum at 60°N, this ITCZ identification procedure has the same effect as searching for the global precipitation maximum, as each of the other experiments has a dominant global precipitation maximum, representing a single ITCZ, at a relatively low latitude. Zonal-mean, time-mean precipitation distributions for each simulation are shown in Figure S3. We define the ITCZ in each simulation to be the latitude of maximum precipitation, though this region bears less dynamical resemblance to Earth's ITCZ in the simulations where the SST maximum is shifted far into the midlatitudes.

2.2. Tropical Cyclone Tracker

TCs were identified and tracked in the model output data using the GFDL TSTORMS tracker (Zhao et al., 2009). At each 6-h time step, the tracker identifies a TC candidate by first identifying a local maximum in relative vorticity at the 850-hPa level that is greater than 3.5×10^{-5} s^{-1}. If a qualifying vorticity maximum is found, the tracker searches for a local minimum in sea-level pressure within 2° of the vorticity maximum. If a qualifying pressure minimum is found, it is identified as the storm center. The tracker searches within 2° of the storm center for a local maximum in the average temperature between the 300-hPa and 500-hPa levels that must be at least 1°C greater than the surrounding mean temperature. If all of the above are found, then they constitute a TC candidate at this time step.

The tracker links TC candidates at successive time steps to form a TC track. If one or more TC candidates are found within 900 km of a TC candidate from the previous time step, then the tracker chooses the closest TC candidate. If the two closest TC candidates are equidistant, preference is given to TC candidates located westward and poleward, to mirror observed TC tracks. If no TC candidate is found within 900 km of a TC candidate from the previous time step, then the track ends. If the track of a TC candidate lasts for at least 3 days and has a surface maximum wind speed of at least 17 m/s on at least three different days, then it is registered as a TC. The tracker outputs the location and maximum 10-m wind speed (v_{max}) of each TC at each time step, allowing analysis of the trajectories, lifetimes, intensities, and frequency of TCs.

3. Linear Regression Model of Tropical Cyclone Frequency

The results of the simulations are shown in Figure 1. The number N of TCs per year and the median TC lifetime τ both exhibit a nonmonotonic dependence on the latitude of the SST maximum. N is close to zero when the SST maximum is near the equator, but N increases sharply as the SST maximum is moved northward from the equator, reaching a maximum when the SST maximum is at 25°N. As the SST maximum is shifted north of 25°N, N decreases but remains relatively high, even when the SST maximum is at 60°N. The median lifetime τ also shows a nonmonotonic dependence, increasing from 3.1 days for the SST maximum at the equator to a maximum of 8.6 days with the SST maximum at 45°N, then decreasing again as the SST maximum is moved farther north.

The mean maximum wind speed of TCs is similar across most simulations, suggesting that the typical TC in each simulation is equally strong. Figure S4 shows additional measures of TC strength: accumulated cyclone energy (ACE) in panels (a–c) and mean minimum pressure (p_{min}) in panel (d). ACE is defined as the sum of the squares of the v_{max} values at each 6-h time step over the lifetime of a TC (Ballinger et al., 2015; Bell et al., 2000), as explained in Text S1. The total annual ACE (Figure S1a) exhibits a similar trend as the trend in N (Figure 1a), and median ACE (Figure S1b) shows a similar trend as the trend in τ (Figure 1b). Like v_{max}, the average TC intensity as represented by $\overline{\text{ACE}}$ (Figure S1c) is overall highly consistent among simulations, again suggesting that the average TC in each simulation is equally strong. This result agrees with our findings that total annual ACE closely follows N and median storm ACE closely follows τ. If the average TC is of relatively consistent strength throughout its lifetime, then the total ACE should be roughly proportional to the number of TCs, and the median ACE should be roughly proportional to the median TC lifetime, just as we find.

The TC frequency in each simulation is modeled as a linear function of the Coriolis parameter at the ITCZ (f_{ITCZ}), weighted by the cosine of the latitude ϕ of the SST maximum, in order to account for the decrease in surface area per degree latitude as one moves poleward. As shown in Figure 2, the linear regression model

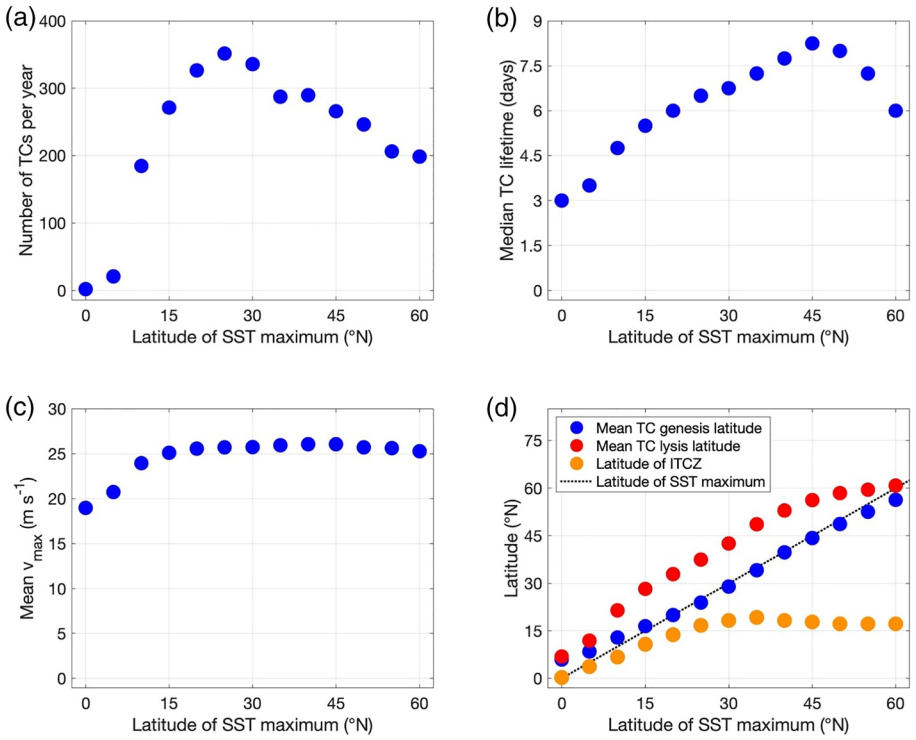

Figure 1. Summary of TC activity across model runs: (a) TC frequency, (b) median TC lifetime, (c) mean maximum wind speed, and (d) mean latitudes of genesis and lysis compared with latitudes of SST maximum and ITCZ. ITCZ, intertropical convergence zone; TC, tropical cyclone.

fits the simulation results accurately, with a correlation coefficient of 0.91. The regression model predictions and simulation results are listed in Table S1. In this regression model, the constant offset is forced to be zero. Allowing a nonzero constant offset improves the correlation coefficient only marginally ($R^2 = 0.911$ vs. $R^2 = 0.908$) and yields a negative constant offset (−4.22), which does not lend itself to physical interpretation.

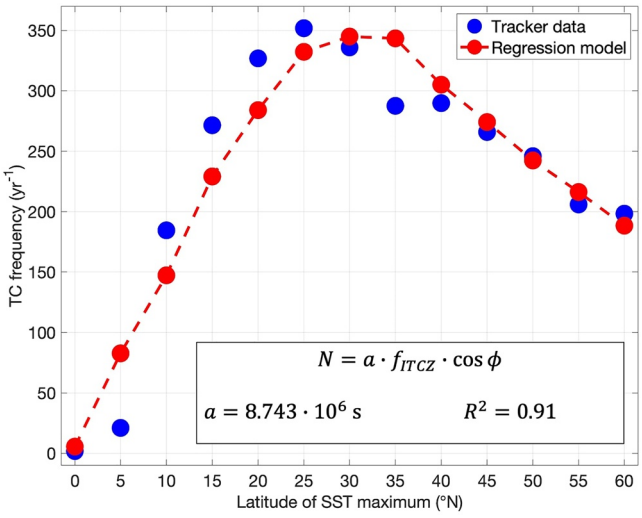

Figure 2. Linear regression of predictors for TC frequency *N*. Blue points show *N* in each simulation, as in Figure 1a. The red points and dashed red line show the predictions of the regression model, where f_{ITCZ} is the Coriolis parameter at the ITCZ and ϕ is the latitude of the SST maximum. ITCZ, intertropical convergence zone; SST, sea surface temperature; TC, tropical cyclone.

As shown in Figure 1d, in the experiments with the SST maximum at low latitudes, the location of the ITCZ closely follows that of the SST maximum. However, as the SST maximum is shifted to higher latitudes, the ITCZ latitude does not keep pace, lagging southward. When the SST maximum is at 30°N, the ITCZ is at approximately 20°N, and it stays within 5° of this latitude for all simulations with the SST maximum farther north.

The physical reasoning underlying the regression model hinges on the idea that in these simulations, TC precursors form as disturbances at the poleward flank of the ITCZ (Ferreira & Schubert, 1997), and more TC precursors spin up when the Coriolis parameter at the ITCZ is larger. Accordingly, we conclude that TC frequency per unit area is a function of f_{ITCZ}. The total TC frequency can be decomposed as follows:

$$\text{TC frequency} = \left(\text{TC frequency per unit area}\right) \times \left(\text{Area of genesis region}\right) \quad (1)$$

As Figure 1d shows, the TC genesis region is around the latitude of maximum SST, so the area of the genesis region is approximately proportional to the cosine of the SST maximum latitude. The area-weighting factor is relatively unimportant at low latitudes, where the cosine function varies slowly. The SST generally must be at least 26.5°C for TC genesis to occur

(e.g., Gray, 1968). As Figure S1 illustrates, the region where the SST satisfies this requirement is centered around the SST maximum latitude and is relatively narrow, with a width of about 4° latitude. Accordingly, it is unsurprising that TC genesis in these simulations occurs close to the latitude of maximum SST. Figure S5 shows zonal profiles of the TC genesis frequency in each simulation, following Merlis et al. (2016) and Chavas and Reed (2019). The ITCZ remains at approximately the same latitude for the simulations with the SST maximum between 35°N and 60°N, as shown in Figure 1f, and the TC genesis frequency per unit area also remains approximately constant, as shown in panels (h–m) of Figure S5. This correspondence visually demonstrates that our physical interpretation of the regression model is reasonable.

Figures S6–S9 show tracks of TCs in four different simulations. To illustrate the mean state, Figure S10 shows zonal-mean zonal wind in each simulation. In most of the simulations, small numbers of TCs form far from the SST maximum, both in the midlatitudes of the southern hemisphere and in the far northern latitudes of the northern hemisphere. Among the 13 simulations, the frequency of these anomalous TCs ranges between 0 and 1.2 per year. These anomalous TCs comprise five of the nine TCs in the experiment with the SST maximum at the equator. Of the remaining four TCs in that experiment, two form at the northern flank of the ITCZ, which is centered at the equator, and the other two form at the southern flank. In all other experiments, the predominant pattern of TC formation is consistent with the physical interpretation of the regression model proposed above.

4. Observed Earth Comparison

We tested the applicability of the linear regression model by applying it to the observed ITCZ position and SST maximum latitude in each basin and month, then comparing the results with the observed TC frequencies. TC frequencies by basin and month were calculated from the International Best Track Archive for Climate Stewardship (IBTrACS; Knapp et al., 2010, Knapp et al., 2018) over the 41-year period from 1979 to 2019, using the "IBTrACS-All" data set of TC tracks recorded by the designated World Meteorological Organization reporting agency for each basin. The basins are defined according to the definitions used in IBTrACS.

The ITCZ position was calculated using Global Precipitation Climatology Project data (GPCP; Adler et al., 2003). The mean global precipitation distribution in each month was calculated from 1979 to 2019. For each of these 12 precipitation distributions, in the region between 20°S and 20°N, the precipitation centroid (Donohoe et al., 2013; Frierson & Hwang, 2012) was calculated at each longitude point, yielding the ITCZ latitude as a function of longitude for each month, which was then used to calculate the mean ITCZ latitude in each basin and month. In making this calculation for each basin, points over land were excluded, and points where the precipitation centroid fell on the opposite side of the equator contributed a value of zero to the average. We use the precipitation centroid to define the ITCZ because it is more robust than the latitude of maximum precipitation, fluctuating less as a function of longitude within each basin. Figure S11 illustrates the basin boundaries and maps the global precipitation distribution and precipitation centroid by month.

The latitude of maximum SST was calculated using Optimum Interpolation Sea Surface Temperature data (OISSTv2; Reynolds et al., 2007). For each month, the mean global SST distribution over the period 1979–2019 was calculated. Using these monthly SST distributions, we calculated the mean latitude of SST greater than 26°C in each basin and month, and used this latitude ϕ for the regression model. (Because the maximum SST occurs at low latitudes for the observed Earth, the area-weighting factor is relatively unimportant, so f_{ITCZ} alone models observed TC frequency relatively accurately.) Figure S12 maps the global SST distribution and latitude ϕ by month. Figure S13 shows the seasonal cycle of the ITCZ and SST maximum latitudes in each basin.

The resulting values of f_{ITCZ} and ϕ are substituted into the proportionality relationship derived from linear regression, using the same proportionality constant a. This analysis yields a prediction of TC frequency in each basin and month. Since the regression model applies to an aquaplanet, these predicted TC frequencies are scaled by the ocean fraction within 20° of the equator in each basin, as well as the fraction of longitude that the basin takes up, to make them comparable with the observed TC frequencies. Figure 3 shows the observed and predicted TC frequencies by month in each basin.

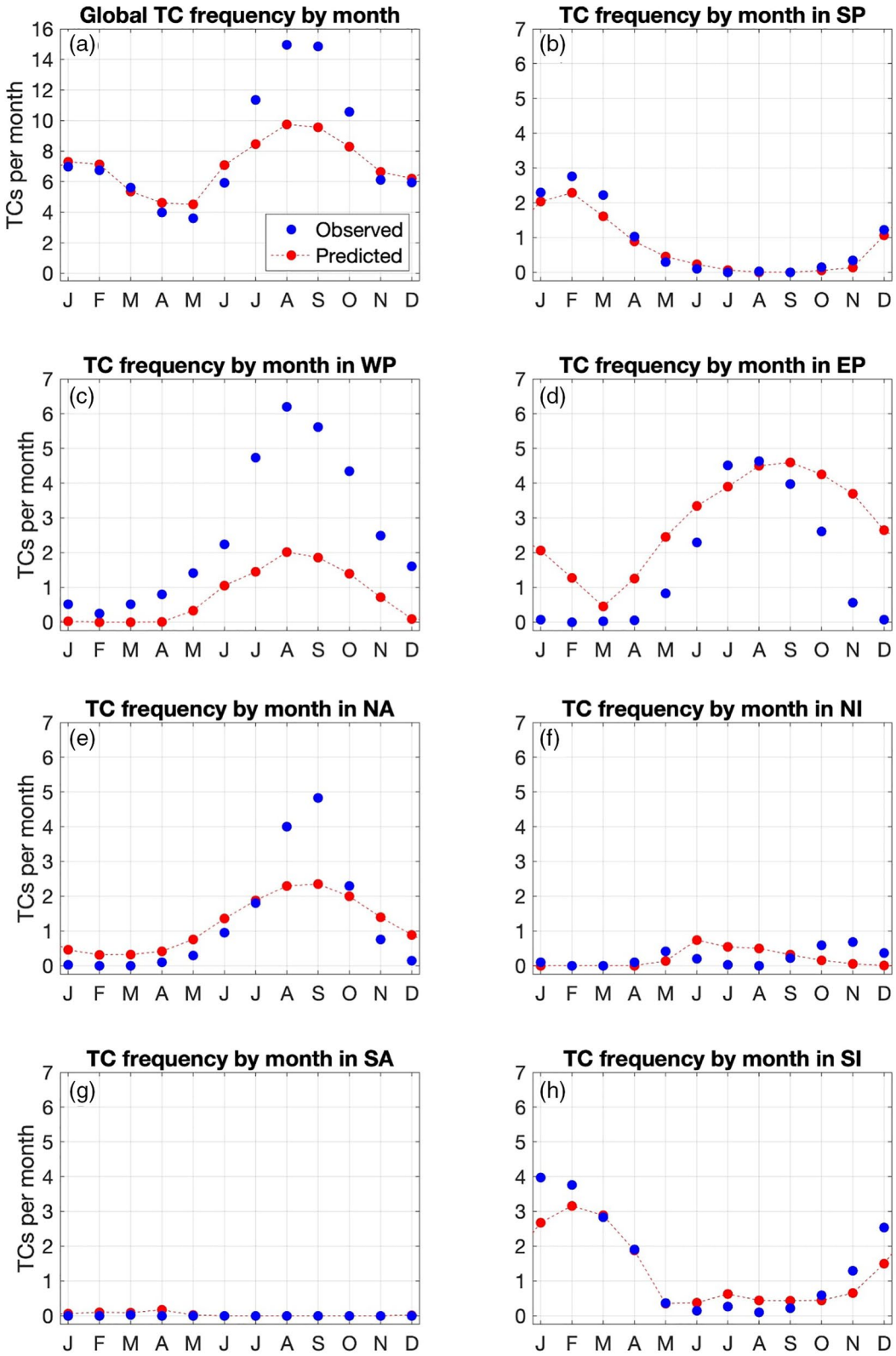

Figure 3. TC frequency observed (blue) and predicted from regression model (red) by month. Panel (a) shows the global TC frequency, computed as the sum of the frequencies in each basin, which are shown in panels (b–h). TC, tropical cyclone.

The total predicted TC frequency is 84.9 per year, whereas the observed frequency is 96.6. As Figure 3a shows, the gap between prediction and observation occurs mainly in July through September; throughout the rest of the year, the observed and predicted global TC frequencies are quite close. These observational results support the conclusion that global TC frequency is a linear function of the Coriolis parameter at the ITCZ. Agreement is best in the South Pacific (SP) basin (Figure 3b), as well as the South Atlantic (SA) basin (Figure 3g), where only one TC was observed during the period 1979–2019 and the predicted TC frequency also remains near zero throughout the year. In the North Atlantic (NA) and South Indian (SI) basins (Figures 3e and 3h), the predicted TC frequency agrees closely with observations throughout much of the year but underestimates the TC frequency at the seasonal peak. In the West North Pacific (WP) basin (Figure 3c), the regression model underpredicts the observed TC frequency throughout the year, whereas in the East North Pacific (EP) basin, the regression model generally overpredicts the TC frequency. The North Indian (NI) basin has a unique bimodal seasonal TC frequency distribution, which is not captured well by this regression model, though the absolute error is small because both the observed and predicted TC frequencies in this basin are low. Proposed dynamical explanations for the varying levels of agreement between the regression model and observations are given in Section 5. One caveat of comparing observed TC frequencies to the TC frequencies predicted by our regression model is that in simulations, absolute numbers of TCs can vary based on GCM resolution and tracking scheme (Shaevitz et al., 2014).

5. Discussion

To our knowledge, this is the first aquaplanet TC study to shift the SST maximum into the midlatitudes. However, the increase in N that occurs as the SST maximum is shifted from the equator to 25°N agrees with the results of Ballinger et al. (2015), who found that N increased as the SST maximum was shifted from 10°N to 16°N. Merlis et al. (2013) found that for small shifts of the ITCZ position, N increased by 40% per degree latitude of northward shift. Rather than specifying the SSTs as a lower boundary condition, that study employed a slab ocean with prescribed cross-equatorial heat flux. Accordingly, our results do not have a direct relationship to their findings, but they are qualitatively similar, lending agreement to the conclusion that the ITCZ position influences N.

Like N, the median TC lifetime τ also shows a nonmonotonic dependence on the latitude of maximum SST, ranging from 3.1 to 8.6 days. Further analysis is needed, but this trend may be explained by the decrease in the β-effect at higher latitudes competing with the decreasing amount of available area for TCs. In most of our simulations, the lifetime of a TC is limited by the amount of time it spends over sufficiently warm SSTs. When β is smaller, the TC moves northward more slowly and therefore spends more time over warm SSTs, so one might expect an increase in TC lifetime as β decreases.

In this study, we define the ITCZ to be the latitude of maximum precipitation. When the SST maximum is at low latitudes, this ITCZ dynamically resembles Earth's ITCZ, and we assume that it provides a source of TC precursors via ITCZ breakdown. We speculate that baroclinic storms may provide an additional source of TC precursors via tropical transition (McTaggart-Cowan et al., 2013), particularly when the SST maximum is shifted into the midlatitudes, but further work is needed to understand the dynamics of TC genesis in these simulations.

In order for our regression model to represent a full physical description of the factors that set TC frequency, the constant coefficient a would need to take on physical meaning of its own. It presumably depends on parameters that were not varied in this study, such as the maximum SST value or the width of the SST distribution. Future idealized modeling studies could perform parameter sweeps of these and other quantities to further constrain the mathematical form of N, following the method used by this study and Ballinger et al. (2015).

Though the regression model applies well to observations in some basins, it is less accurate in others. In the WP basin, precipitation plots show a double ITCZ, with one branch on each side of the equator. Our calculation of the latitude of this double-branched ITCZ is biased toward the equator, because it involves taking the centroid, then taking the mean of the centroid points on each side of the equator. Accordingly, this method underestimates the value of f at the northern branch of the ITCZ in the WP basin, and thus underestimates the TC frequency, as shown in Figure 3c. The southern branch of the ITCZ at these longitudes lies in the SP

basin, but it is close to the equator, so our calculation of f_{ITCZ} here remains relatively accurate. Additionally, the SP basin has a wide longitudinal extent, so when f_{ITCZ} is averaged over this basin, the effect of the double ITCZ in the westernmost reaches of this basin is muted. In most of the eastern portion of this basin, plots of precipitation show that there is no ITCZ, and the calculated value of f_{ITCZ} is zero.

In the NA basin, the observed frequency of TCs during peak TC season, July and August, is about double what is predicted based on f_{ITCZ}. We speculate that sources of TC precursors other than the ITCZ instability, such as African easterly waves (e.g., Russell et al., 2017), account for these additional observed TCs. Our regression model slightly overestimates the TC frequency from November through June, when there are few or no TCs in the NA basin. During these months, even though f_{ITCZ} is nonzero, we assume TC genesis is impeded by other factors not considered in our regression model, such as high vertical shear or insufficiently high SSTs.

In conclusion, we find that the key factor controlling TC frequency per unit area in this study is the Coriolis parameter f at the ITCZ. This advance in understanding TC frequency on an aquaplanet represents a new step toward a large-scale dynamical theory of TC frequency, and toward the prospect of robust predictions of TC frequency under climate change. Previous studies have identified the Coriolis parameter (Chavas & Reed, 2019) and climatic controls on formation of TCs from TC precursors (Vecchi et al., 2019) as fundamental dynamical determinants of the rate of TC genesis. Future work will employ further idealized modeling studies in an effort to determine additional ingredients of a large-scale dynamical theory for TC frequency.

Conflict of Interest

The authors declare no conflicts of interest relevant to this study.

Data Availability Statement

The TSTORMS software is available for download at <https://www.gfdl.noaa.gov/tstorms/>, and AM4.0 is available for download at <https://data1.gfdl.noaa.gov/nomads/forms/am4.0/>. SST distributions used to force the model are described in the text and illustrated in the supporting information. The IBTrACS data used for the observed Earth comparison are publicly available through the indicated reference. GPCP data also are publicly available, provided by the NOAA/OAR/ESRL PSL, Boulder, Colorado, USA, at <https://psl.noaa.gov/data/gridded/data.gpcp.html>. The OISST data are publicly available at <https://climatedataguide.ucar.edu/climate-data/sst-data-noaa-high-resolution-025x025-blended-analysis-daily-sst-and-ice-oisstv2>. The analysis of observational data involved use of the MATLAB "landmask" function by Chad Greene, available at <mathworks.com/matlabcentral/fileexchange/48661-landmask>.

Acknowledgments
We thank Isaac Held, Tim Merlis, and Adam Sobel for productive discussions. We thank Daniel Chavas for his detailed reviews. We also thank a second, anonymous reviewer. This work was partly funded by the National Science Foundation (NSF) through grant AGS-1921409 to Stanford University. L. G. Silvers acknowledges support through Stony Brook University from NSF award AGS-1830729.

References

Adler, R. F., Huffman, G. J., Chang, A., Ferraro, R., Xie, P., Janowiak, J., et al. (2003). The version 2 Global Precipitation Climatology Project (GPCP) monthly precipitation analysis (1979-present). *Journal of Hydrometeorology*, *4*, 1147–1167. https://doi.org/10.1175/1525-7541(2003)004<1147:TVGPCP>2.0.CO;2

Ballinger, A. P., Merlis, T. M., Held, I. M., & Zhao, M. (2015). The sensitivity of tropical cyclone activity to off-equatorial thermal forcing in aquaplanet simulations. *Journal of the Atmospheric Sciences*, *72*, 2286–2302. https://doi.org/10.1175/JAS-D-14-0284.1

Bell, G. D., Halpert, M. S., Schnell, R. C., Higgins, R. W., Lawrimore, J., Kousky, V. E., et al. (2000). Climate assessment for 1999. *Bulletin of the American Meteorological Society*, *81*, S1–S50. https://doi.org/10.1175/1520-0477(2000)81[s1:CAF]2.0.CO.2

Byrne, M. P., Pendergrass, A. G., Rapp, A. D., & Wodzicki, K. R. (2018). Response of the intertropical convergence zone to climate change: Location, width, and strength. *Current Climate Change Reports*, *4*(4), 355–370. https://doi.org/10.1007/s40641-018-0110-5

Camargo, S. J., Emanuel, K. A., & Sobel, A. H. (2007). Use of a genesis potential index to diagnose ENSO effects on tropical cyclone genesis. *Journal of Climate*, *20*, 4819–4834. https://doi.org/10.1175/JCLI4282.1

Camargo, S. J., Tippett, M. K., Sobel, A. H., Vecchi, G. A., & Zhao, M. (2014). Testing the performance of tropical cyclone genesis indices in future climates using the HiRAM model. *Journal of Climate*, *27*(24), 9171–9196. https://doi.org/10.1175/JCLI-D-13-00505.1

Chavas, D. R., & Reed, K. A. (2019). Dynamical aquaplanet experiments with uniform thermal forcing: system dynamics and implications for tropical cyclone genesis and size. *Journal of the Atmospheric Sciences*, *76*(8), 2257–2274. https://doi.org/10.1175/JAS-D-19-0001.1

Donohoe, A., Marshall, J., Ferreira, D., & Mcgee, D. (2013). The relationship between ITCZ location and cross-equatorial atmospheric heat transport: From the seasonal cycle to the Last Glacial Maximum. *Journal of Climate*, *26*, 3597–3618. https://doi.org/10.1175/JCLI-D-12-00467.1

Emanuel, K. A. (1986). An air-sea interaction theory for tropical cyclones. Part I: Steady-state maintenance. *Journal of the Atmospheric Sciences*, *43*, 585–605. https://doi.org/10.1175/1520-0469(1986)043<0585:AASITF>2.0.CO.2

Emanuel, K. A. (2006). Climate and tropical cyclone activity: A new model downscaling approach. *Journal of Climate*, *19*, 4797–4802. https://doi.org/10.1175/JCLI3908.1

Emanuel, K. A. (2013). Tropical cyclones in CMIP5 simulations. *Proceedings of the National Academy of Sciences*, *110*(30), 12219–12224. https://doi.org/10.1073/pnas.1301293110

Eyring, V., Bony, S., Meehl, G. A., Senior, C. A., Stevens, B., Stouffer, R. J., & Taylor, K. E. (2016). Overview of the Coupled Model Intercomparison Project Phase 6 (CMIP6) experimental design and organization. *Geoscientific Model Development*, *9*, 1937–1958. https://doi.org/10.5194/gmd-9-1937-2016

Ferreira, R. N., & Schubert, W. H. (1997). Barotropic aspects of ITCZ breakdown. *Journal of the Atmospheric Sciences*, *54*, 261–285. https://doi.org/10.1175/1520-0469(1997)054<0261:BAOIB>2.0.CO.2

Frierson, D. M. W., & Hwang, Y. (2012). Extratropical influence on ITCZ shifts in slab ocean simulations of global warming. *Journal of Climate*, *25*, 720–733. https://doi.org/10.1175/JCLI-D-11-00116.1

Gray, W. M. (1968). Global view of the origin of tropical disturbances and storms. *Monthly Weather Review*, *96*(10), 669–700. https://doi.org/10.1175/1520-0493(1968)096<0669:GVOTOO>2.0.CO.2

Harris, L. M., & Lin, S.-J. (2013). A two-way nested global-regional dynamical core on the cubed-sphere grid. *Monthly Weather Review*, *141*, 283–306. https://doi.org/10.1175/MWR-D-11-00201.1

Held, I. M., & Zhao, M. (2011). The response of tropical cyclone statistics to an increase in CO_2 with fixed sea surface temperatures. *Journal of Climate*, *24*, 5353–5364. https://doi.org/10.1175/JCLI-D-11-00050.1

Hsieh, T.-L., Vecchi, G. A., Yang, W., Held, I. M., & Garner, S. T. (2020). Large-scale control on the frequency of tropical cyclones and seeds: a consistent relationship across a hierarchy of global atmospheric models. *Climate Dynamics*, *55*(11), 3177–3196. https://doi.org/10.1007/s00382-020-05446-5

Knapp, K. R., Kruk, M. C., Levinson, D. H., Diamond, H. J., & Neumann, C. J. (2010). The International Best Track Archive for Climate Stewardship (IBTrACS): Unifying tropical cyclone best track data. *Bulletin of the American Meteorological Society*, *91*, 363–376. https://doi.org/10.1175/2009BAMS2755.1

Knapp, K. R., Diamond, H. J., Kossin, J. P., Kruk, M. C., & Schreck, C. J. (2018). *International best track archive for climate stewardship (IBTrACS) project, version 4*. NOAA National Centers for Environmental Information. https://doi.org/10.25921/82ty-9e16

McTaggart-Cowan, R., Galarneau, T. J., Bosart, L. F., Moore, R. W., & Martius, O. (2013). A global climatology of baroclinically influenced tropical cyclogenesis. *Monthly Weather Review*, *141*(6), 1963–1989. https://doi.org/10.1175/MWR-D-12-00186.1

Merlis, T. M., & Held, I. M. (2019). Aquaplanet simulations of tropical cyclones. *Current Climate Change Reports*, *5*, 185–195. https://doi.org/10.1007/s40641-019-00133-y

Merlis, T. M., Zhao, M., & Held, I. M. (2013). The sensitivity of hurricane frequency to ITCZ changes and radiatively forced warming in aquaplanet simulations. *Geophysical Research Letters*, *40*, 4109–4114. https://doi.org/10.1002/grl.50680

Merlis, T. M., Zhou, W., Held, I. M., & Zhao, M. (2016). Surface temperature dependence of tropical cyclone-permitting simulations in a spherical model with uniform thermal forcing. *Geophysical Research Letters*, *43*, 2859–2865. https://doi.org/10.1002/2016GL067730

Möbis, B., & Stevens, B. (2012). Factors controlling the position of the intertropical convergence zone on an aquaplanet. *Journal of Advances in Modeling Earth Systems*, *4*, M00A04. https://doi.org/10.1029/2012MS000199

Neale, R. B., & Hoskins, B. J. (2000). A standard test for AGCMs including their physical parametrizations: I. The proposal. *Atmospheric Science Letters*, *1*, 101–107. https://doi.org/10.1006/asle.2000.0022

Putman, W. M., & Lin, S.-J. (2007). Finite-volume transport on various cubed-sphere grids. *Journal of Computational Physics*, *227*(1), 55–78. https://doi.org/10.1016/j.jcp.2007.07.022

Reynolds, R. W., Smith, T. M., Liu, C., Chelton, D. B., Casey, K. S., & Schlax, M. G. (2007). Daily high-resolution-blended analyses for sea surface temperature. *Journal of Climate*, *20*, 5473–5496. https://doi.org/10.1175/2007JCLI1824.1

Russell, J. O., Aiyyer, A., White, J. D., & Hannah, W. (2017). Revisiting the connection between African Easterly Waves and Atlantic tropical cyclogenesis. *Geophysical Research Letters*, *44*, 587–595. https://doi.org/10.1002/2016GL071236

Shaevitz, D. A., Camargo, S. J., Sobel, A. H., Jonas, J. A., Kim, D., Kumar, A., et al. (2014). Characteristics of tropical cyclones in high-resolution models in the present climate. *Journal of Advances in Modeling Earth Systems*, *6*, 1154–1172. https://doi.org/10.1002/2014MS000372

Williamson, D. L., Blackburn, M., Hoskins, B. J., Nakajima, K., Ohfuchi, W., Takahashi, Y. O., et al. (2012). *The APE atlas, NCAR technical note NCAR/TN-484+STR, xxii+508*. Boulder, CO: National Center for Atmospheric Research. https://doi.org/10.5065/D6FF3QBR

Vecchi, G. A., Delworth, T. L., Murakami, H., Underwood, S. D., Wittenberg, A. T., Zeng, F., et al. (2019). Tropical cyclone sensitivities to CO2 doubling: roles of atmospheric resolution, synoptic variability and background climate changes. *Climate Dynamics*, *53*, 5999–6033. https://doi.org/10.1007/s00382-019-04913-y

Zhao, M., & Held, I. M. (2012). TC-permitting GCM simulations of hurricane frequency response to sea surface temperature anomalies projected for the late twenty-first century. *Journal of Climate*, *25*, 2995–3009. https://doi.org/10.1175/JCLI-D-11-00313.1

Zhao, M., Held, I. M., Lin, S., & Vecchi, G. A. (2009). Simulations of global hurricane climatology, interannual variability, and response to global warming using a 50-km resolution GCM. *Journal of Climate*, *22*, 6653–6678. https://doi.org/10.1175/2009JCLI3049.1

Zhao, M., Golaz, J.-C., Held, I. M., Guo, H., Balaji, V., Benson, R., et al. (2018a). The GFDL global atmosphere and land model AM4.0/LM4.0: 1. Simulation characteristics with prescribed SSTs. *Journal of Advances in Modeling Earth Systems*, *10*, 691–734. https://doi.org/10.1002/2017MS001208

Zhao, M., Golaz, J.-C., Held, I. M., Guo, H., Balaji, V., Benson, R., et al. (2018b). The GFDL global atmosphere and land model AM4.0/LM4.0: 2. Model description, sensitivity studies, and tuning strategies. *Journal of Advances in Modeling Earth Systems*, *10*, 735–769. https://doi.org/10.1002/2017MS001209